NUCLEAR THEORY, Vol. 42 (2025)
eds. M. Gaidarov, N. Minkov, Heron Press, Sofia

Advancing the Microscopic Relativistic Description of Nuclear Excitations: From Second Tamm-Dancoff Approximation to Second Random Phase Approximation

D. Vale[1], **N. Paar**[2],

[1]Istrian University of Applied Sciences, Preradovieva ulica 9D, 52100 Pula, Croatia
[2]Department of Physics, Faculty of Science, University of Zagreb, Bijenička cesta 32, 10000 Zagreb, Croatia

Abstract. A detailed understanding of nuclear collective excitations and astrophysical processes necessitates theoretical approaches that surpass the limitations of the Random Phase Approximation (RPA). While RPA has been instrumental in describing small-amplitude oscillations in nuclei, its simplicity, rooted in the 1-particle–1-hole ($1p$–$1h$) configuration space, leads to its limitations to account for the fragmentation of nuclear strength, the spreading width, and the neglect of multi-particle correlations crucial for describing higher-order phenomena. To resolve these limitations, we have recently developed and applied a fully self-consistent relativistic Second Tamm-Dancoff Approximation (RSTDA) and Second Random Phase Approximation (RSRPA) framework, which incorporates 2-particle–2-hole ($2p$–$2h$) configurations. Both methods aregrounded in relativistic nuclear energy density functional theory, providing a microscopic foundation for the description of nuclear excitations. Our work focuses on the fragmentation of isoscalar and isovector monopole and quadrupole transitions in ^{16}O, ^{40}Ca, and ^{48}Ca. The subtraction method was employed to consistently eliminate double-counting effects and infrared divergence. We explored the impact of the subtraction method by comparing results with and without its application in both RSRPA and RSTDA. Preliminary SRPA results for selected transitions provide a perspective for further analysis of higher-order correlations. These findings emphasize the importance of complex configurations and the subtraction method in achieving a detailed microscopic description of nuclear collective phenomena.

1 Introduction

The theoretical description of collective nuclear excitations is essential for understanding fundamental properties of atomic nuclei and their role in various astrophysical processes. Standard approaches, such as the relativistic Random phase approximation (RRPA) and relativistic Tamm-Dancoff approximationx (RTDA), are limited to one-particle–one-hole ($1p$–$1h$) configurations [1, 2].

These models are capable of describing certain low-lying states and the gross features of giant resonances. However, they cannot fully account for experimentally observed phenomena such as the fragmentation of transition strength, spreading widths, and the presence of complex correlations, particularly in light nuclei and exotic systems [3–7].

To overcome these limitations, theoretical frameworks have been developed that extend beyond the simple $1p$–$1h$ configuration space [8–15]. In our recent works, we introduced the relativistic second Tamm-Dancoff approximation (RSTDA), which incorporates two-particle–two-hole ($2p$–$2h$) configurations within the relativistic point-coupling energy density functional [16–18]. The subtraction method was implemented to eliminate double counting of correlations, ensuring a consistent coupling between simple and complex configurations [17,18]. Applications of the RSTDA to isoscalar monopole and quadrupole transitions in ^{16}O demonstrated improved description of fragmentation and fine structure of the nuclear response [17]. Nevertheless, the RSTDA framework remains limited by neglecting backward-going amplitudes and certain dynamical correlations that are essential for a complete treatment of nuclear excitations.

More recently, we have taken the next step by introducing the relativistic Second Random Phase Approximation (RSRPA) [19]. By including both forward- and backward-going amplitudes, the RSRPA enables a fully correlated treatment of $1p$–$1h$ and $2p$–$2h$ configurations. This provides a more realistic description of damping mechanisms and the microscopic origins of spreading widths in giant resonances. Moreover, the relativistic formulation guarantees self-consistency between ground-state correlations and excited states, in accordance with the principles of covariant density functional theory and the underlying symmetries of quantum chromodynamics (QCD).

In this work, we investigate the microscopic mechanisms driving strength fragmentation and spreading within the diagonal approximation of the relativistic RSTDA and the RSRPA. We apply the newly developed RSTDA framework to the study of isoscalar giant monopole resonances (ISGMR) and isoscalar giant quadrupole resonances (ISGQR) in ^{16}O, ^{40}Ca, and ^{48}Ca within limited configuration spaces. By systematically comparing the results obtained with RTDA, the diagonal approximation of RSTDA(d), and its subtracted counterpart, i.e., RSSTDA(d), the study investigates the characteristics of giant resonances, including the energy spectra, strength distributions, and fragmentation patterns. For the diagonal approximation of RSRPA (RSRPA(d)) and its subtracted version (RSSRPA(d)), we have presented only illustrative results for the ISGMR and IVGMR in ^{40}Ca, in order to draw a parallel with STDA and to facilitate a comparison of the obtained results (see also Ref. [18]).

While the present study is limited to the diagonal approximation, the full form of RSRPA, both with and without the subtraction procedure, has been recently developed and applied to ^{16}O in a study [19]. For ^{40}Ca and ^{48}Ca, only preliminary results have been obtained and analyzed in the larger configuration space, including the influence of couplings between two-particle–two-hole ($2p$–

$2h$) configurations, which will be addressed in future work. Such developments will allow for a more comprehensive description of nuclear excitations and provide a solid foundation for the study of open-shell nuclei and astrophysically relevant nuclear processes.

2 Theoretical Framework

2.1 From Thouless theorem to RSRPA equations

Standard approaches for description of nuclear excitations, based solely on $1p$–$1h$ configurations, often are insufficient to capture the complexity of nuclear dynamics, especially in the presence of collective modes and higher-order correlations. To properly account for the coupling between single-particle states and more complex excitations, the conventional Thouless operator must be generalized. In this extended framework, the excited Slater determinant includes contributions not only from $1p$–$1h$ and 1α–$1h$, but also from $2p$–$2h$ configurations [8]. This leads to a generalized excitation operator of the form [17]

$$\hat{Z}(t) = \sum_{ph} Z^{(1)}_{ph}(t)\, a^\dagger_p a_h + \sum_{\alpha h} Z^{(1)}_{\alpha h}(t)\, a^\dagger_\alpha a_h + \frac{1}{4} \sum_{pp'hh'} Z^{(2)}_{pp'hh'}(t)\, a^\dagger_p a^\dagger_{p'} a_{h'} a_h, \quad (1)$$

where the first two terms describe the usual $1p$–$1h$ and 1α–$1h$ excitations (the symbol α denotes states from the Dirac sea of negative energies), while the last term explicitly incorporates two-particle-two-hole correlations ($2p$–$2h$), enabling a more comprehensive treatment of complex nuclear configurations.

The complete time-dependent wave function of the quantum system can be constructed by acting with the generalized excitation operator $\hat{Z}$ on the ground state. The expression of the full wave function is then given by [19]

$$|\Phi(t)\rangle = \exp\left(\hat{Z}(t)\right)|\Phi_0\rangle. \quad (2)$$

The equations of motion for the time-dependent excitation amplitudes $Z^{(1)}_{ph}(t)$, $Z^{(1)}_{\alpha h}(t)$, and $Z^{(2)}_{pp'hh'}(t)$ are obtained within the framework of the time-dependent variational principle. Following the strategy outlined in our recent work [19], we employ a symmetrized version of the Dirac-Frenkel variational approach, which has been shown to provide a consistent treatment of correlations beyond the standard RPA level [19]. In this formalism, the dynamics of the system is determined by imposing that the action functional remains stationary under small variations of the excitation amplitudes. The action is defined as [19]

$$\mathcal{S}[Z^{(1)}, Z^{(2)}, c.c.] = \frac{1}{2}\int dt(\langle\Phi(t)|i\partial_t - \hat{H}|\Phi(t)\rangle + \langle\Phi(t)|-i\overleftarrow{\partial_t} - \hat{H}|\Phi(t)\rangle), \quad (3)$$

where $\hat{H}$ is the many-body relativistic Hamiltonian of the system and $|\Phi(t)\rangle$ is the wave function introduced in Eq. (2). This framework naturally extends beyond the RPA by incorporating both one- and two-particle-two-hole configurations within a unified description of collective nuclear excitations.

After carrying out the variational procedure and simplifying the resulting expressions, the equations of motion can be recast into a compact and more familiar matrix form [19]:

$$\begin{pmatrix} A & B \\ -B^* & -A^* \end{pmatrix} \begin{pmatrix} X \\ Y \end{pmatrix} = \hbar\omega \begin{pmatrix} X \\ Y \end{pmatrix}, \tag{4}$$

where A and B matrix contain the following blocks:

$$A = \begin{pmatrix} A_{11} & A_{12} \\ A_{21} & A_{22} \end{pmatrix}, \quad \text{and} \quad B = \begin{pmatrix} B_{11} & B_{12} \\ B_{21} & B_{22} \end{pmatrix}. \tag{5}$$

This matrix representation corresponds to the SRPA framework, which extends the standard RPA by incorporating not only the residual interactions within the individual subspaces, but also the explicit coupling between the $1p$–$1h$ (1α–$1h$) and $2p$–$2h$ configurations. Detailed expressions for the matrix elements of all blocks of the A and B matrices, which also account for the rearrangement contributions, are provided in the Refs. [17, 19]. When the matrix B vanishes, the (R)SRPA equations reduce to the (R)STDA form.

2.2 DD-PC1 parametrization of Lagrangian

Relativistic energy density functionals with density-dependent point-coupling interactions provide a consistent basis for nuclear structure calculations. Including the free-nucleon and electromagnetic components, the Lagrangian density takes the form [20, 21]:

$$\begin{aligned} \mathcal{L} \; = & \bar{\psi}\left(i\gamma_\mu\partial^\mu - m\right)\psi - \frac{1}{2}\alpha_S(\rho)\left(\bar{\psi}\psi\right)\left(\bar{\psi}\psi\right) \\ & - \frac{1}{2}\alpha_V(\rho)\left(\bar{\psi}\gamma_\mu\psi\right)\left(\bar{\psi}\gamma^\mu\psi\right) - \frac{1}{2}\alpha_{TV}(\rho)\left(\bar{\psi}\vec{\tau}\gamma_\mu\psi\right)\left(\bar{\psi}\vec{\tau}\gamma^\mu\psi\right) \\ & - \frac{1}{2}\delta_S\partial_\nu\left(\bar{\psi}\psi\right)\partial^\nu\left(\bar{\psi}\psi\right) - e\bar{\psi}\gamma_\mu A^\mu\frac{1-\tau_3}{2}\psi. \end{aligned} \tag{6}$$

In this formulation, the density dependence is explicitly included in the case of the isoscalar-scalar $\alpha_S(\rho)$, isoscalar-vector $\alpha_V(\rho)$ and isovector-vector coupling $\alpha_{TV}(\rho)$ as

$$\alpha_i\left[x\right] \; = \; a_i + (b_i + c_i x)\exp(-d_i x), \tag{7}$$

where $x = \rho/\rho_{sat}$, ρ stands for barion (vector) density and ρ_{sat} for the nucleon density at saturation in the symmetric nuclear matter [20, 21]. In this work, the DD-PC1 parametrization is adopted [21].

2.3 Transition strength

In order to investigate collective spin-independent modes within the RSRPA, the external field operator F is defined as:

$$\begin{aligned} \hat{F}^{\mathrm{IS}}_{\lambda M} &= \sum_i r_i^k Y_{\lambda M}(\Omega_i), \\ \hat{F}^{\mathrm{IV}}_{\lambda M} &= \sum_i r_i^k Y_{\lambda M}(\Omega_i)\hat{t}_z(i), \end{aligned} \tag{8}$$

for the isoscalar (IS) and isovector (IV) channel, respectively. For the monopole operator, $\lambda = 0$ and $k = 2$, while for the quadrupole operator $\lambda = 2$ and $k = 2$. The strength distribution associated with this operator is defined as

$$S_F(\omega) = \sum_\nu |\langle\nu|\hat{F}|0\rangle|^2 \, \delta(\omega - \omega_\nu), \tag{9}$$

where $|\nu\rangle$ are the excited states obtained by solving the (R)SRPA eigenvalue problem, and ω_ν are the corresponding excitation energies.

The transition matrix element is then computed as

$$\langle\nu|\hat{F}|0\rangle = \sum_{ph}\left(f_{ph}X^{(1)\nu}_{ph} + f_{hp}Y^{(1)\nu}_{ph}\right) + \sum_{\alpha h}\left(f_{\alpha h}X^{(1)\nu}_{\alpha h} + f_{h\alpha}Y^{(1)\nu}_{\alpha h}\right), \tag{10}$$

where $f_{ph} = \langle p|\hat{f}|h\rangle$ are the single-particle transition matrix elements of the operator $\hat{f}$. The $2p$-$2h$ states do not contribute at this order, as the one-body operator $\hat{F}$ cannot connect them directly to the reference state $|\Phi_0\rangle$. In the RSTDA case, Eq. (10) consists only of forward-going (X) amplitudes.

2.4 Subtracted form of diagonal SSRPA

The subtraction procedure was carried out following Ref. [14], while the matrix formulations for the diagonal case of the subtracted RSRPA (RSSRPA(d)) were based on our previous work [17]:

$$\begin{aligned} \mathcal{A}^S_D &= \begin{pmatrix} A_{11'} + \sum_2 A_{12}(A^{\mathrm{diag}}_{22})^{-1}A_{21'} + \sum_2 B_{12}(A^{\mathrm{diag}}_{22})^{-1}B_{21'} & A_{12} \\ A_{21} & A^{\mathrm{diag}}_{22} \end{pmatrix}, \\ \mathcal{B}^S_D &= \begin{pmatrix} B_{11'} + \sum_2 A_{12}(A^{\mathrm{diag}}_{22})^{-1}B_{21'} + \sum_2 B_{12}(A^{\mathrm{diag}}_{22})^{-1}A_{21'} & B_{12} \\ B_{21} & 0 \end{pmatrix}. \end{aligned} \tag{11}$$

For the (R)SSTDA(d), the previous expression simplifies to

$$\begin{aligned} \mathcal{A}^S_D &= \begin{pmatrix} A_{11'} + \sum_2 A_{12}\left(A^{\mathrm{diag}}_{22}\right)^{-1}A_{21'} & A_{12} \\ A_{21} & A^{\mathrm{diag}}_{22} \end{pmatrix}, \\ \mathcal{B}^S_D &= 0. \end{aligned} \tag{12}$$

3 RSTDA and RSSTDA Results

3.1 ISGMR and ISGQR

Figure 1 presents the Lorentz-smoothed strength distributions for the ISGMR and ISGQR in ^{16}O, ^{40}Ca, and ^{48}Ca, obtained using the RSTDA(d) and RSSTDA(d) approaches. For all calculations, the major quantum number was consistently set to $N = 8$ to allow for a straightforward comparison across different nuclei and approaches. The RTDA results are included for reference, providing a baseline for assessing the improvements introduced by the extended formalism.

The ISGMR strength distributions for all approaches in ^{16}O lie almost entirely above the experimental centroid energy (21.13 MeV [3]), indicating that the major quantum number $N = 8$ is insufficient for an accurate description in this nucleus. For ^{40}Ca and ^{48}Ca, both RSTDA and RSSTDA(d) yield centroid energies that are in good agreement with the experimental values (19.18 MeV [4] and 19.88 MeV [6]), although somewhat larger downward shifts of

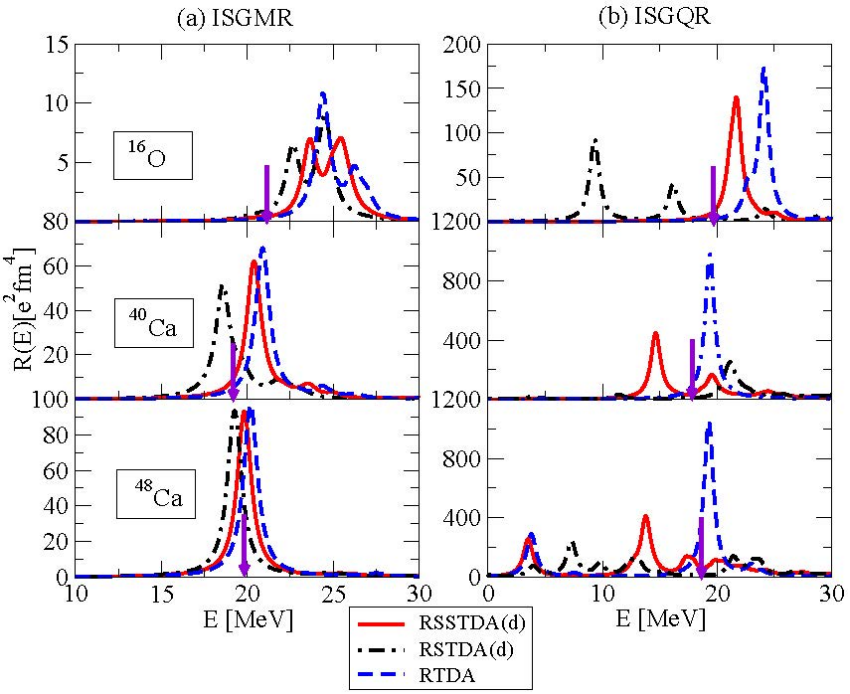

Figure 1. Lorentzian-smoothed isoscalar GMR and GQR strength distributions in ^{16}O, ^{40}Ca and ^{48}Ca calculated using the RSTDA(d), RSSTDA(d), and RTDA. Part of the results, namely the ISGQR in ^{16}O and ^{40}Ca and the ISGMR in ^{40}Ca, have been reported earlier in [18]. The arrows indicate the experimental centroid energies for each mode [3, 4, 6].

the peaks are observed in the case of RSTDA(d). Specifically, for the ISGMR in ^{40}Ca, the centroid energies amount to 21.06 MeV in RSSTDA(d) [18] and 21.55 MeV in RTDA, while in ^{48}Ca the corresponding values are 20.15 MeV and 20.41 MeV, respectively. On the other hand, the RSSTDA(d) shifts in the ISGMR spectrum exhibit a weak energy dependence, tending to converge for $2p$–$2h$ cutoff values above 120–140 MeV in ^{40}Ca or ^{16}O and above ≈ 110 MeV in ^{48}Ca.

In contrast, for the ISGQR in ^{40}Ca, the RSTDA(d) response shows a significant downward shift of the peak energies, and for $2p$–$2h$ cutoff values exceeding 100 MeV, parts of the spectrum even enter the unphysical negative-energy region. For ^{16}O and ^{48}Ca, pronounced shifts of the peak energies are observed. Nevertheless, in both cases, the strength distribution remains entirely within the physical (positive-energy) region, even for high $2p$–$2h$ energy cutoff values up to 200 MeV in ^{16}O and up to 100 MeV in ^{48}Ca. In the case of the ISGQR in ^{40}Ca, the centroid energy predicted by the RSSTDA(d) approach (18.88 MeV [18]) shows improved agreement with the experimental value (17.84 MeV), compared to the RTDA result (19.59 MeV). A similar trend is observed for ^{48}Ca, where the centroid energy obtained with RSSTDA(d) (18.54 MeV) is closer to the experimental value (18.61 MeV) than the RTDA result (19.77 MeV). For details on other moments and the width of the distribution in ^{16}O and ^{40}Ca, the reader is referred to Ref. [18].

These observations demonstrate the intrinsic limitations of the RSTDA(d) approach and highlight the importance of employing the RSSTDA(d) to achieve a more reliable and physically consistent description of both the monopole and quadrupole responses.

3.2 Infrared divergence

Figure 2 illustrates the calculated discrete ISGQR strength distributions in ^{40}Ca, providing insight into the impact of different theoretical approaches on the excitation spectrum. The RSSTDA(d) results show a more stable spectrum with peaks concentrated at specific energies, indicating improved convergence. In contrast, the RSTDA(d) spectrum exhibits additional fragmented peaks, particularly at lower excitation energies, reflecting stronger mixing and reduced stability. This behavior can be interpreted as a manifestation of an infrared divergence in a broader sense, associated with the sensitivity of low-energy states to the cutoff and configuration space. The RTDA solution differs significantly from both of the mentioned RSRPA approaches. For the chosen $2p$–$2h$ cutoff, the RSTDA(d) shows eigenvalue shifts of up to 30 MeV relative to the RTDA reference, with some eigenvalues even dropping deeply into the negative excitation-energy region, where they lack a clear physical interpretation. In contrast, in RSSTDA(d) these shifts are much more localized, remaining within approximately 5 MeV. Furthermore, when compared to the experimental centroid energy for ^{40}Ca (17.84 MeV [4]), the lowest state obtained within RTDA lies at a higher energy than the experimental centroid.

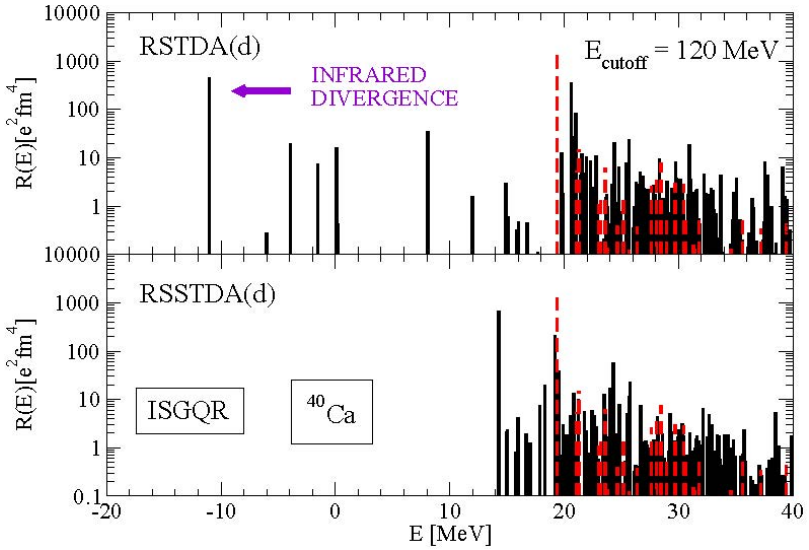

Figure 2. Comparison of discrete ISGQR strength distributions in ^{40}Ca, calculated using the RSTDA(d) and RSSTDA(d) with a $2p$–$2h$ energy cutoff of $E_{\mathrm{cutoff}} = 120$ MeV. The standard TDA result is included in both panels as red dashed lines for reference.

4 RSRPA and RSSRPA Results

As an illustrative example of the excitation spectrum description, we consider the ISGMR and IVGMR in ^{40}Ca (see Figure 3), calculated using two approaches, i.e., RSRPA(d) and RSSRPA(d). In these calculations, a major oscillator quantum number of $N = 8$ was employed. The RSRPA(d) results exhibit a systematic downward shift of the eigenvalues with increasing configuration space. For small cutoff energies, the shift is of the order of a few hundred keV, while for cutoff values above approximately 120 MeV the shift reaches several MeV. In contrast, the RSSRPA(d) approach demonstrates significantly greater stability, i.e., the eigenvalues display only minor displacements up to ≈ 1 MeV and tend to converge as the cutoff energy exceeds 120 MeV. This behavior highlights the improved robustness of the RSSRPA(d) formalism in describing collective monopole excitations and its suitability for reliable predictions of giant resonance properties.

5 Conclusion

In this study, we have presented selected results obtained using the RSTDA(d) and its subtracted counterpart (RSSTDA(d)) for the doubly magic nuclei ^{16}O, ^{40}Ca, and ^{48}Ca. The present analysis has focused on the energy spectrum and excitation properties of the ISGMR and the ISGQR within a limited configura-

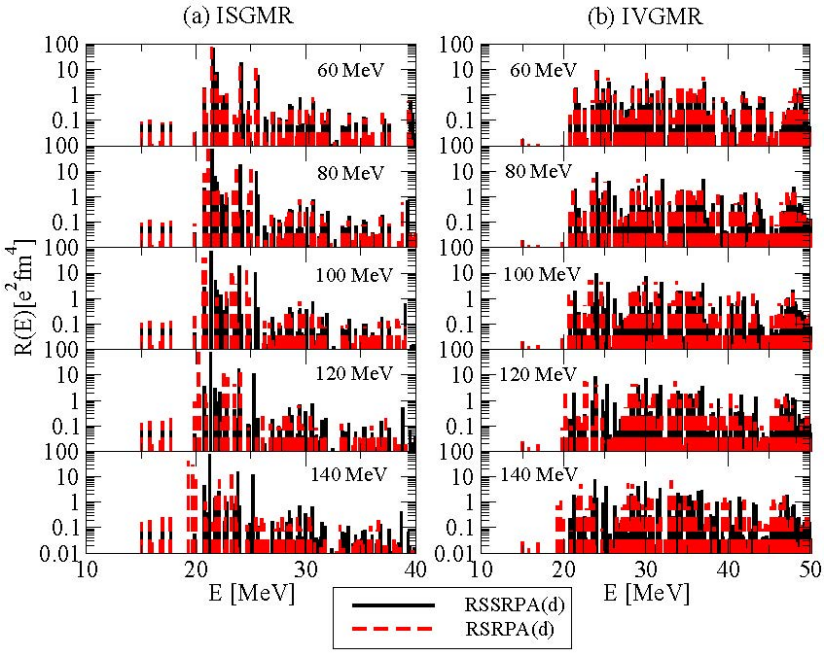

Figure 3. Discrete (a) ISGMR and (b) IVGMR strength distributions in ^{40}Ca calculated for different $2p$-$2h$ cutoff energies using the RSRPA(d) and RSSRPA(d). The sequence of subplots corresponds to increasing $2p$–$2h$ cutoff values, demonstrating how the response evolves as additional configurations are taken into account.

tion space. A more detailed investigation, including the full implementation of the RSTDA and RSSTDA, using larger configuration space, was performed for ^{16}O and reported in Ref. [17], while the corresponding analysis for ^{40}Ca and ^{48}Ca is in progress.

Particular attention was given to the ISGQR, where the occurrence of the infrared divergence in the RSTDA(d) framework was investigated. This divergence leads to unphysical shifts of the excitation spectrum towards lower energies, and in many cases even to negative energies, especially when larger $2p$–$2h$ energy cutoffs are employed.

In addition, we have presented the first results of the RSRPA in the diagonal approximation, both with and without the subtraction procedure, for the ISGMR in ^{40}Ca. It was observed that the RSRPA exhibits trends similar to those previously reported for the RSTDA in recent works [17, 18]. These findings indicate that the diagonal approximation within the RSRPA framework inherits the same infrared instabilities as the RSTDA, and further emphasize the importance of implementing the subtraction procedure to obtain a physically consistent description of the collective nuclear response.

A detailed comparative analysis of the diagonal RSTDA and RSRPA is beyond the scope of the present work and will be addressed in a forthcoming study.

Acknowledgements

This work was supported by the Croatian Science Foundation under the project Relativistic Nuclear Many-Body Theory in the Multimessenger Observation Era (HRZZ-IP-2022-10-7773).

References

[1] N. Paar, P. Ring, T. Nikšić, D. Vretenar, *Phys. Rev. C* **67** (2003) 034312.
[2] N. Paar, T. Nikšić, D. Vretenar, P. Ring, *Phys. Rev. C* **69** (2004) 054303.
[3] Y.-W. Lui, H.L. Clark, D.H. Youngblood, *Phys. Rev. C* **64** (2001) 064308.
[4] D.H. Youngblood, Y.-W. Lui, H.L. Clark, *Phys. Rev. C* **63** (2001) 067301; [Erratum: *Phys. Rev. C* **64** (2001) 049901].
[5] T. Hartmann, J. Enders, P. Mohr, K. Vogt, S. Volz, A. Zilges, *Phys. Rev. C* **65** (2002) 034301.
[6] Y.-W. Lui, D.H. Youngblood, S. Shlomo, X. Chen, Y. Tokimoto, Krishichayan, M. Anders, J. Button, *Phys. Rev. C* **83** (2011) 044327.
[7] K.B. Howard, U. Garg, M. Itoh, H. Akimune, S. Bagchi, T. Doi, Y. Fujikawa, M. Fujiwara, T. Furuno, M.N. Harakeh, Y. Hijikata, K. Inaba, S. Ishida, N. Kalantar-Nayestanaki, T. Kawabata, S. Kawashima, K. Kitamura, N. Kobayashi, Y. Matsuda, A. Nakagawa, S. Nakamura, K. Nosaka, S. Okamoto, S. Ota, S. Weyhmiller, Z. Yang, *Phys. Lett. B* **801** (2020) 135185.
[8] J. Da Providência, *Nucl. Phys.* **61** (1965) 87-96.
[9] P. Papakonstantinou, R. Roth, arXiv:0709.3167 [nucl-th] (2007).
[10] P. Papakonstantinou, R. Roth, *Phys. Rev. C* **81** (2010) 024317.
[11] D. Gambacurta, M. Grasso, F. Catara, *Phys. Rev. C* **81** (2010) 054312.
[12] D. Gambacurta, M. Grasso, F. Catara, *J. Phys. G: Nucl. Part. Phys.* **38** (2011) 035103.
[13] D. Gambacurta, M. Grasso, V. De Donno, G. Co', F. Catara, *Phys. Rev. C* **86** (2012) 021304.
[14] D. Gambacurta, M. Grasso, J. Engel, *Phys. Rev. C* **92** 034303 (2015).
[15] F. Minato, *Phys. Rev. C* **93** (2016) 044319.
[16] D. Vale, N. Paar, *Nucl. Theory* **41** (2024) 2-10.
[17] D. Vale, N. Paar, *Phys. Rev. C* **112** (2025) 034327.
[18] D. Vale, N. Paar, *The first applications of the relativistic Second Tamm-Dancoff approximation in doubly-magic nuclei*, Web of Conferences, manuscript under review (2025).
[19] D. Vale, G. Saxena, and N. Paar, *Relativistic Second Random-Phase Approximation: Formalism and Applications to Giant Resonances*, manuscript in preparation (2025).
[20] T. Nikšić, N. Paar, D. Vretenar, P. Ring, *Comp. Phys. Comm.* **185** (2014) 1808.
[21] T. Nikšić, D. Vretenar, P. Ring, *Phys. Rev. C* **78** (2008) 034318.